Electrocardiographic Imaging of Sinus Rhythm in Pig Hearts using Bayesian Maximum A Posteriori Estimation

Y. Serinagaoglu Dogrusoz[1], R. Dubois[2], E Abell[2], M. Cluitmans[3], L. R. Bear[2],
[1]Electrical-Electronics Engineering Dept, Middle East Technical University, Ankara,Turkey
[2]IHU-LIRYC, Université de Bordeaux, Bordeaux, France
[3]Maastricht University, Maastricht, The Netherlands

Abstract

Background: *Electrocardiographic imaging (ECGI) has potential to guide physicians to plan treatment strategies. Previously, Bayesian maximum a posteriori (MAP) estimation has been successfully applied to solve this inverse problem for paced data. In this study, we evaluate its effectiveness using experimental data in reconstructing sinus rhythm.* **Methods:** *Four datasets from Langendorff-perfused pig hearts, suspended in a human-shaped torso-tank, were used. Each experiment included 3-5 simultaneous electrogram (EGM) and body surface potential (BSP) recordings of 10 beats, in baseline and under dofetilide and pinacidil perfusion. Bayesian MAP estimation and Tikhonov regularization were used to solve the inverse problem. Prior models in MAP were generated using beats from the same recording but excluding the test beat. Pearson's correlation was used to evaluate EGM reconstructions, activation time (AT) maps, and gradient of ATs.* **Results:** *In almost all quantitative evaluations and qualitative comparisons of AT maps and epicardial breakthrough sites, MAP outperformed substantially better than Tikhonov regularization.* **Conclusion:** *These preliminary results showed that with a "good" prior model, MAP improves over Tikhonov regularization in terms of preventing misdiagnosis of conduction abnormalities associated with arrhythmogenic substrates and identifying epicardial breakthrough sites.*

1. Introduction

Noninvasive electrocardiographic imaging (ECGI) is a novel tool that aims to reconstruct cardiac electrical sources using body-surface potential (BSP) measurements and a patient-specific mathematical model relating the sources to the measurements [1]. This inverse problem is ill-posed due to attenuation and smoothing of the potentials within the thorax. Methods such as Tikhonov regularization [2] are applied to stabilize the solutions and obtain accurate reconstructions.

ECGI has great potential as a clinical tool for guiding ablation therapy of cardiac arrhythmias, and revealing the mechanisms underlying various cardiac electrical disorders [3]. However, variability in the spatio-temporal behavior of the electrograms (EGM) shortcomings of traditional regularization methods for capturing these details limit the accuracy of identifying arrhythmogenic substrates in sinus rhythm with these widely applied ECGI methods [4]. Current ECGI methods (Tikhonov regularization included) have been found to incorrectly identify abnormalities in conduction associated with arrhythmogenic substrates, such as artefactual conduction slowing and block [5]. Furthermore, these methods have also been found to reduce the number of epicardial breakthrough sites and poorly localize them, falsely suggesting that abnormalities in the Purkinje system exist that could trigger arrhythmia in these patients. Improvement of ECGI methods for the accurate reconstruction of epicardial exit sites and conduction slowing is imperative if ECGI is to be used to identify the mechanisms underlying major electrical diseases, and for subsequent arrhythmia risk stratification.

Previously, Bayesian maximum a posteriori (MAP) estimation has been successfully applied to ECGI for localizing pacing sites for paced data [6]. In this study, we evaluated its effectiveness in reconstructing sinus rhythm from experimental data. Sinus rhythm is known to result in artifacts using standard ECGI methods [5]. We applied MAP estimation, assuming jointly Gaussian EGM and BSPs. Measurement noise was assumed to be Gaussian, independent, and identically distributed (iid). Tikhonov regularization was also used for comparison.

2. Experimental Data

The experimental protocol for the acquisition of the data used in this study has previously been described [7] and is summarized below. All experimental procedures were approved by the Directive 2010/63/EU of the European Parliament on the protection of animals used for scientific purposes and the local ethical committee.

Four hearts from Langendorff-perfused *ex-vivo* pig hearts were suspended in a human-shaped torso-tank with 256 embedded electrodes. EGMs were recorded via 108-lead sock electrodes simultaneously with the

Table 1. Summary of all quantitative metrics.

Exp No	Intervention	EGM-CC Median(IQR)		AT-CC Median(IQR)		gradAT-CC Median(IQR)	
		MAP	Tikhonov	MAP	Tikhonov	MAP	Tikhonov
1	Baseline	0.74(0.02)	0.60(0.02)	0.98(0.00)	0.92(0.01)	0.53(0.04)	0.20(0.01)
	Drug	0.80(0.00)	0.63(0.01)	0.99(0.00)	0.93(0.00)	0.60(0.01)	0.17(0.03)
	All	**0.77(0.06)**	**0.61(0.03)**	**0.99(0.00)**	**0.93(0.00)**	**0.57(0.06)**	**0.19(0.03)**
2	Baseline	0.76(0.06)	0.70(0.03)	0.75(0.25)	0.87(0.04)	0.29(0.16)	0.22(0.03)
	Drug	0.75(0.02)	0.67(0.08)	0.90(0.01)	0.88(0.02)	0.29(0.06)	0.21(0.13)
	All	**0.74(0.03)**	**0.69(0.06)**	**0.88(0.09)**	**0.88(0.03)**	**0.29(0.12)**	**0.21(0.03)**
3	Baseline	0.65(0.09)	0.51(0.08)	0.85(0.03)	0.68(0.04)	0.31(0.01)	0.08(0.04)
	Drug	0.61(0.00)	0.53(0.04)	0.85(0.00)	0.67(0.01)	0.35(0.00)	0.05(0.00)
	All	**0.61(0.09)**	**0.53(0.07)**	**0.85(0.03)**	**0.67(0.03)**	**0.32(0.03)**	**0.06(0.05)**
4	Baseline	0.68(0.07)	0.59(0.05)	0.77(0.14)	0.46(0.04)	0.32(0.20)	0.05(0.02)
	Drug	0.70(0.01)	0.57(0.00)	0.82(0.01)	0.72(0.01)	0.19(0.01)	0.11(0.01)
	All	**0.70(0.07)**	**0.57(0.05)**	**0.82(0.13)**	**0.49(0.26)**	**0.22(0.21)**	**0.07(0.06)**

corresponding BSPs (BioSemi, the Netherlands) at 2 kHz during sinus rhythm. Each experiment included 3-5 recordings of 10 beats, in baseline and under dofetilide and pinacidil perfusion (drugs that alter action potential duration). 3D rotational fluoroscopy (Artis, Siemens) was used to obtain the position of the epicardium and electrodes with respect to the torso tank after the completion of the experiments.

3. Methods

The relationship between the EGMs and BSPs are expressed as:

$$\mathbf{y} = \mathbf{A}\mathbf{x} + \mathbf{n} \qquad (1)$$

at each time instant, where $\mathbf{y} \in \mathbf{R}^M$, $\mathbf{x} \in \mathbf{R}^N$, $\mathbf{n} \in \mathbf{R}^M$ and $\mathbf{A} \in \mathbf{R}^{M \times N}$ are the BSPs, EGMs, measurement noise and the forward matrix, respectively.

The boundary element method was used to solve the forward problem employing a homogeneous conductivity between the epicardial mesh (1088 nodes, 2172 triangles) and a refined tank surface mesh (4002 nodes, 8000 triangles) [8]. The rows of the resulting forward matrix corresponding to the 256 torso electrode locations were then subsampled to define **A.**

Bayesian MAP estimation is a statistical approach, in which the epicardial potentials and the noise are treated as random [6]. The posterior probability density function (pdf) of the EGM is defined based on the likelihood function of the measurements, $p(\mathbf{y}\backslash\mathbf{x})$, and an *a priori* pdf, $p(\mathbf{x})$, modelling available prior information on the EGMs as:

$$p(\mathbf{x}\backslash\mathbf{y}) = \frac{p(\mathbf{y}\backslash\mathbf{x})p(\mathbf{x})}{\int p(\mathbf{y}\backslash\mathbf{x})p(\mathbf{x})d\mathbf{x}} \qquad (2)$$

The MAP solution maximizes this posterior pdf. A detailed explanation of the method can be found in [6]. We

assumed that the EGMs and BSPs are jointly Gaussian; $\mathbf{x} \sim N(\bar{\mathbf{x}}, \mathbf{C_x})$, $\mathbf{n} \sim N(\mathbf{0}, \sigma_n^2\mathbf{I})$, and $\mathbf{n}$ is uncorrelated with $\mathbf{x}$.

The mean $\bar{\mathbf{x}}$ and the covariance matrix $\mathbf{C_x}$ were estimated for each beat using a leave-one-beat-out protocol; for each experiment and intervention, one beat is used as the test beat and the remaining 9 beats constitute the training data.

Tikhonov zero-order regularization was also applied for comparison with the Bayesian MAP estimation results. The L-curve method was used to define the regularization parameter [9].

For each test beat, ECGI reconstructions were compared quantitatively with the sock recordings at the corresponding 108 nodes in terms of Pearson's correlation coefficient (EGM-CC). Activation times (AT) were calculated for the recorded and reconstructed EGMs using the maximum negative derivative method, and the spatio-temporal method proposed in [10], respectively. We also computed the gradient of the ATs (gradAT) as the difference in AT of each edge of the mesh, divided by the length of the edge. This was used to reveal when line of block (LOB) may be occurring in the ground truth EGMs and ECGI reconstructions. Pearson's correlation was used to compare ATs and spatial gradients of ATs. The higher gradAT-CC, the less likely ECGI has accidently created a LOB artefact where it does not exist (i.e., there is no LOB in the ground truth ATs). We also investigated the number and localization error of the epicardial breakthroughs as additional evaluation criteria.
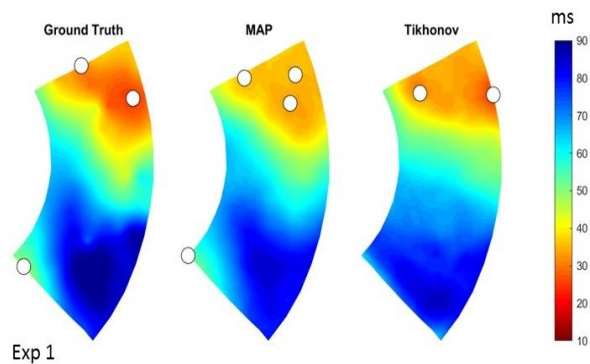
4. Results

Table 1 summarizes the median and interquartile range (IQR) values for EGM-CC, AT-CC, and gradAT-CC for all datasets and interventions.

In all metrics, MAP had substantially better performance than Tikhonov. There was 8% (from 0.70 to
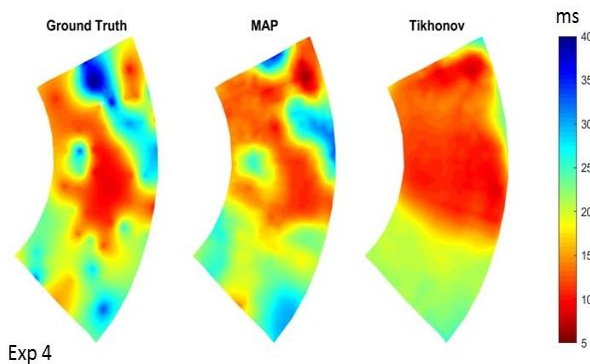
Figure 1. Baseline AT map for Exp 4.

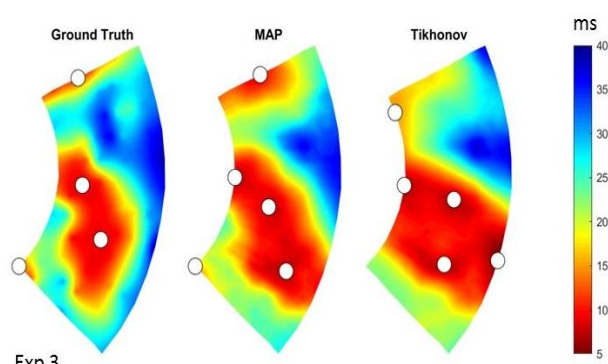Figure 2. Baseline AT map for Exp 1.

0.76) - 27% (from 0.63 to 0.80 and from 0.51 to 0.65) increase in median EGM-CC, and 2% (from 0.88 to 0.90) - 67% (from 0.46 to 0.77) increase in median AT-CC in the MAP results compared to Tikhonov. In one case only (exp 2, baseline), median AT-CC of MAP dropped by 14% (from 0.87 to 0.75).

MAP had gradAT-CC values that were substantially higher than (exp 1, 3 and 4) or similar to (exp 2) Tikhonov regularization, suggesting that when a "good" prior is chosen we can reduce the appearance of conduction abnormalities in the reconstruction.

Example AT maps are presented in Figures 1-4, along with the estimated epicardial breakthrough locations (white circles) for the last three examples. In these figures, the sock electrodes, which are wrapped around the ventricles of the heart, are shown unwrapped for a complete view of the heart surface. Left and right sides correspond to the apex and base, and the lower and upper regions are the left (LV) and the right (RV) ventricles.

The example in Figure 1 demonstrates a ground truth AT map with a complicated activation wavefront. There were slow conduction regions as seen by closely neighboring early and late activated areas. These details were completely missed by the Tikhonov regularization. MAP showed a far better performance in capturing the details of these true AT maps.

In Figure 2, the AT map obtained by MAP had better
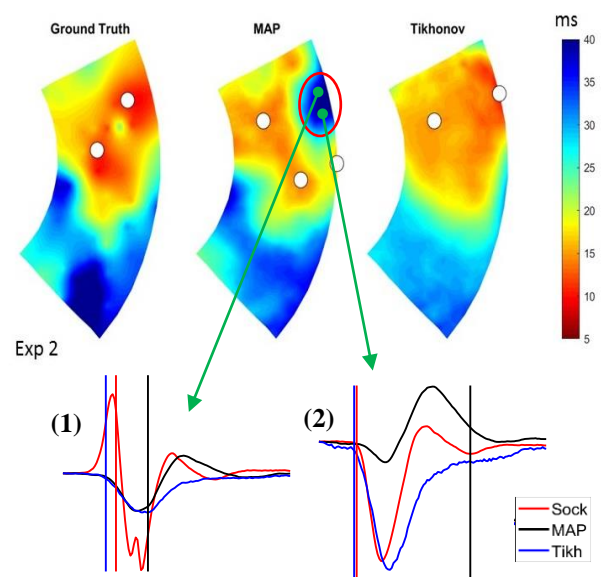

Figure 3. Baseline AT map for Exp 3.

Figure 4. Baseline AT map for Exp 2, along with the sock and reconstructed EGMs at two nodes from the MAP reconstructions with late AT.

fidelity to the ground truth than the Tikhonov regularization; the latter over-smoothed the AT maps. As a result, the epicardial breakthrough in the lower left corner (located at the LV apex) is missed by the Tikhonov AT reconstruction, but captured by MAP. This could result in the false diagnosis of left bundle branch block (LBBB) with the Tikhonov-based ECGI.

In Figure 3, Tikhonov AT reconstructions are better than in the previous two examples; general distribution and the presence of epicardial breakthroughs on both LV and RV regions are in agreement with the ground truth AT and MAP AT reconstruction. Still, the AT map of Tikhonov is oversmoothed compared to MAP and the location of epicardial breakthroughs are inaccurate.

The last example shown in Figure 4 is from experiment 2, in which the AT-CC for MAP is worse than Tikhonov. MAP reconstructs late activated areas, which are not present in the ground truth. Sock and reconstructed EGMs

were also shown for two leads from this area. In lead (1), although the MAP and Tikhonov reconstructions are similar early in the QRS, the AT is incorrectly estimated for MAP. In lead (2), reconstructed EGM with MAP has a smaller peak-to-peak amplitude compared to the sock and Tikhonov EGMs. The same over-smoothing by Tikhonov is still observed in this example; complicated activation wavefront in the lower region of the RV-LV boundary is better captured by MAP than Tikhonov.

5.   Discussion

In almost all quantitative evaluations and qualitative AT map comparisons, MAP performed substantially better than Tikhonov regularization. The only exception was in one of the baseline recordings of exp 2 (Figure 4), in which the AT computation was incorrect for MAP even though the EGMs reconstructions were accurate.

Examination of the epicardial breakthroughs revealed that Tikhonov tended to merge close breakthroughs into a single large early site (Figure 1), underestimate the number of breakthroughs (Figure 2), or shift their location (Figure 3). MAP for the most part captured all breakthroughs, though on occasion an extra breakthrough would appear close to existing breakthroughs (Figures 2 and 3). These breakthroughs demonstrated a similar or better localization error to those reconstructed with Tikhonov. Of particular interest, the number of outliers with large localization errors were substantially reduced with MAP (mean LE of 14 mm versus 18 mm with Tikhonov over all datasets).

Analysis was only performed in pig hearts with normal conduction; the drugs used in this study tend to alter action potential duration, but typically have no impact on conduction. Further analysis of the changes in repolarization using this data is underway, and assessment of reconstructions using data from pig hearts with conduction abnormalities is needed.

In this study, we used a "good" prior model for MAP, where the statistical model parameters are estimated from the data coming from the same heart as the test data. Our work continues on incorporating simulated EGMs for the estimation of the prior model.

5.   Conclusions

These preliminary results showed that with a "good" prior model, MAP improves over Tikhonov regularization in terms of preventing misdiagnosis of conduction abnormalities associated with arrhythmogenic substrates and identifying epicardial breakthrough sites.

Acknowledgements

References

[1] Cluitmans MJM, Peeters RLM, Westra RL, Volders PGA. Noninvasive reconstruction of cardiac electrical activity: update on current methods, applications and challenges. Neth Heart J 2015;23:301–311.

[2] Tikhonov AN, Arsenin VY. Solutions of ill-posed problems. Halsted Press, NY, 1977.

[3] Dubois R, Shah AJ, Hocini M, Denis A, Derval N, Cochet H, Sacher F, Bear L, Duchateau J, Jais P, Haissaguerre M. Non-invasive cardiac mapping in clinical practice: Application to the ablation of cardiac arrhythmias. Journal of electrocardiology. 2015;48(6):966-74.

[4] Bear LR, LeGrice IJ, Sands GB, Lever NA, Loiselle DS, Paterson DJ, Cheng LK, Smaill BH. How Accurate Is Inverse Electrocardiographic Mapping?: A Systematic In Vivo Evaluation. Circulation: Arrhythmia and Electrophysiology. 2018;11(5):e006108.

[5] Duchateau J, Sacher F, Pambrun T, Derval N, Chamorro-Servent J, Denis A, Ploux S, Hocini M, Jaïs P, Bernus O, Haïssaguerre M, Dubois R. Performance and limitations of noninvasive cardiac activation mapping. *Heart Rhythm* 2019;

[6] Serinagaoglu Y, Brooks DH, MacLeod RS. Bayesian solutions and performance analysis in bioelectric inverse problems. IEEE Transactions on Biomedical Eng June 2005; 52(6):1009–1020.

[7] Bear LR, Huntjens PR, Walton RD, Bernus O, Coronel R, Dubois R. Cardiac electrical dyssynchrony is accurately detected by noninvasive electrocardiographic imaging. Heart rhythm. 2018;15(7):1058-69.

[8] Ramanathan C, Rudy Y. Electrocardiographic imaging: II. Effect of torso inhomogeneities on noninvasive reconstruction of epicardial potentials, electrograms, and isochrones. J. Cardiac Electrophys. 2001:12(2) 241–52.

[9] Hansen PC, O'Leary DP. The use of the L-curve in the regularization of discrete ill-posed problems. SIAM Journal on Scientific Computing. 1993;14(6):1487-503.

[10] Erem B., Coll-Font J., Orellana R. M., Stovicek P., Brooks D. H. (2014) Using transmural regularization and dynamic modeling for noninvasive cardiac potential imaging of endocardial pacing with imprecise thoracic geometry. IEEE Trans. on Med. Imag., 33(3), 726-738.

Dr. Yesim Serinagaoglu Dogrusoz
Orta Dogu Teknik Universitesi
Elektrik and Elektronik Muh. Bol.
Ankara, Turkey
yserin@metu.edu.tr